Microsecond time-scale dynamics from relaxation in the rotating frame: experiments using spin lock with alternating phase

Ivan S. Podkorytov and Nikolai R. Skrynnikov[*]

Department of Chemistry, Purdue University, West Lafayette, IN 47907-2084, USA

Abstract

A spin lock comprised of radiofrequency pulses with alternating phase, $(x)(-x)(x)(-x)\ldots$, is proposed as a new technique to probe microsecond time-scale dynamics. A series of $R_{1\rho}$ measurements using different pulse duration t_p allows one to determine exchange rate, k_{ex}, the product $p_a p_b (\Delta\omega_{ab})^2$ involving populations of the exchanging species, p_a and p_b, together with chemical shift difference, $\Delta\omega_{ab}$, and the strength of the spin-lock field, B_1. The interpretation is based on simple analytical expression for $R_{1\rho}$ derived on the basis of Redfield theory. The application of the method is demonstrated for partially deuterated molecule of cyclohexane undergoing chair-to-chair interconversion at $-9\,°C$.
© 2004 Elsevier Inc. All rights reserved.

Keywords: NMR; Relaxation; Rotating frame of reference; Spin lock; $T_{1\rho}$; Chemical exchange; µs to ms time scale; Cyclohexane; Protein dynamics

1. Introduction

NMR spectroscopy is a unique method for probing microsecond-to-millisecond time scale motions at atomic level resolution. Many dynamic processes that fall in this range are of primary interest for organic, organometallic, and biological chemistry. For example, in the context of protein studies NMR techniques were recently used to probe ligand binding [1,2], protein folding [3], and enzymatic catalysis [4].

Information about µs to ms dynamics is obtained from broadening of spectral lines. This effect can be interpreted in a general manner using the master equation for spin density matrix supplemented with an exchange superoperator [5]. In the important case of fast dynamics, exchange broadening can be described by Redfield theory and expressed as a relaxation contribution due to stochastic modulation of isotropic chemical shift, R_{ex} [6]. Redfield-type analyses have been carried out for various motional models including multi-site exchange [7] and in the context of multi-spin systems [8].

Fast-to-intermediate time-scale chemical exchange can be most readily studied using the dependence of R_{ex} on the strength of the applied radiofrequency (RF) field. Two basic experimental schemes have been employed so far toward this goal: (i) continuous-wave spin lock with constant amplitude and phase [6] and (ii) Carr–Purcell–Meiboom–Gill (CPMG) train of hard 180° pulses [9]. The first experiment is usually interpreted in the rotating frame of reference where the energy levels of the spin-1/2 system are separated by $\hbar\omega_1$ (ω_1 represents the strength of the spin-lock field). The increase in ω_1 widens the gap between the energy levels. As a result, the stochastic motion becomes less efficient in causing relaxation transitions between the said energy levels. This effect manifests itself through the Redfield-theory spectral density, $J(\omega_1) = \int_0^\infty d\tau G(\tau)\exp(-i\omega_1\tau)$. In the case when correlation function $G(\tau)$ has simple exponential form [7], $J(\omega_1)$ declines monotonically with ω_1. The resulting dependence of R_{ex} on ω_1 is known as the "relaxation dispersion curve."

Considering the CPMG approach, the argument can be made that 180° pulses refocus the chemical shift evolution and thus prevent the build-up of randomly modulated phase which is the basis of exchange broadening [10]. Introducing the effective RF field associated

[*] Corresponding author. Fax: 1-765-494-0239.
E-mail address: nikolai@purdue.edu (N.R. Skrynnikov).

with the train of pulses, $\omega_1^{\text{eff}} = \pi/\zeta$, where ζ is the delay between the two consecutive pulses, one can observe that R_{ex} declines with increase in ω_1^{eff}, similar to the case of continuous-wave spin lock.

It is useful to summarize the expressions for exchange-induced relaxation rates measured in the two experiments for a single spin exchanging between two non-equivalent sites:

$$R_{1\rho}^{\text{CW}} = p_a p_b (\Delta\omega_{ab})^2 \tau_{\text{ex}} \left[\frac{1}{1 + (\omega_1 \tau_{\text{ex}})^2} \right], \tag{1}$$

$$R_{1\rho}^{\text{CPMG}} = p_a p_b (\Delta\omega_{ab})^2 \tau_{\text{ex}} \left[1 - \frac{2\omega_1^{\text{eff}} \tau_{\text{ex}}}{\pi} \tanh \frac{\pi}{2\omega_1^{\text{eff}} \tau_{\text{ex}}} \right]. \tag{2}$$

Here $\tau_{\text{ex}} = 1/(k_{ab} + k_{ba})$ is the correlation time of the exchange process expressed through the direct, k_{ab}, and reverse, k_{ba}, exchange rates, and p_a and $p_b = 1 - p_a$ are the populations of the states a and b. The results of Eqs. (1), (2) are valid when $\Delta\omega_{ab}\tau_{\text{ex}} \ll 1$. This condition asserts the validity of Redfield approach and corresponds to the fast exchange regime when a single spectral line is observed at the frequency $\omega_{\text{obs}} = p_a\omega_a + p_b\omega_b$. The results are given for an on-resonance case when the carrier is set at ω_{obs}.

Here we suggest that both spin-lock and CPMG experiments can be viewed as representatives of the broad class of rotating-frame experiments employing amplitude and phase-modulated RF fields. Another experiment that falls in this general category is adiabatic spin lock introduced by Tollinger and Konrat [11]. All these experiments are suitable for studies of μs to ms time scale chemical exchange. The philosophy of this approach is briefly outlined below (cf. discussion of time-dependent spin Hamiltonians by Goldman [12]).

Let us assume that the amplitude of the RF field is time-dependent, $\omega_1 = \omega_1(t)$. The Redfield-theory treatment of spin relaxation leads then to the generalized form of spectral density $K = \int_0^\infty d\tau G(\tau) \exp(-i \int_{t-\tau}^t \omega_1(t') dt')$ (see Appendix A, Eq. (A.6), for details). The exponential factor in the expression for K can be expressed in terms of Fourier transform, $\exp(-i \int_{t-\tau}^t \omega_1(t') dt') = \int_{-\infty}^\infty S(\tilde\omega_1, t) \exp(-i\tilde\omega_1\tau) d\tilde\omega_1$. Note that non-trivial Fourier spectrum $S(\tilde\omega_1, t)$ reflects modulation of the energy levels arising from time-dependent $\omega_1(t)$. Making the substitution in the expression for K and reversing the order of integration one obtains $K = \int_{-\infty}^\infty S(\tilde\omega_1, t)J(\tilde\omega_1) d\tilde\omega_1$. Thus, K can be viewed as the generalized spectral density that encodes multiple spectral components of the correlation function $G(\tau)$. It also can be described as *polychromatic* spectral density in contrast to *monochromatic* $J(\omega_1)$ which encodes a single spectral component of the correlation function.

In practice, the amplitude of the RF field, $\omega_1(t)$, can be varied on the time scale of several microseconds. This

is fast compared to the exchange rates of interest (τ_{ex} is in μs to ms range). This situation can be contrasted with relaxation experiments in the laboratory frame. For obvious technical reasons, Zeeman frequency ω_0 cannot be changed on the scale of typical correlation times (ps to ns). The fact that the external field $\omega_1(t)$ can be rapidly varied on the time scale of the correlation time makes the generalized spectral density K an interesting new object within the framework of Redfield theory.

In this paper we present the experiment for relaxation measurements in the rotating frame employing *alternating-phase (AP) spin lock*. This experiment can be viewed as another member of the general class of relaxation dispersion experiments discussed above. The theoretical treatment of the AP spin-lock experiment leads to closed analytical expression along the lines of Eqs. (1,2). The results are confirmed by experimental measurements on a sample of cyclohexane undergoing chair-to-chair transformation. It is demonstrated that the scheme can potentially have a number of practical advantages.

2. Results and discussion

A simple pulse sequence employing spin lock with alternating phase, $(x)(-x)(x)(-x)\ldots(x)(-x)$, is shown in Fig. 1. The spectral properties of the $(x)(-x)$ pulse train have been previously used for spin decoupling [13] and Hartmann–Hahn magnetization transfer [14]. In our experiment, alternating-phase spin lock is used as a new probe for μs time-scale dynamics. The spin-lock period in the pulse sequence Fig. 1 is comprised of pulses of duration t_p separated by short service delays δ (necessary for clean phase-switching). The total duration of the spin-lock period formed in this manner is $T = 2N(t_p + \delta)$. The last pulse before the acquisition period plays the role of the purging pulse (necessary for instrumental reasons as discussed later).

As in the case of the original spin-lock studies [6], our experiment is aimed at the spin systems in the fast exchange regime, $\Delta\omega_{ab}\tau_{\text{ex}} \ll 1$, where two exchanging species give rise to a single spectral line at the frequency $\omega_{\text{obs}} = p_a\omega_a + p_b\omega_b$. The relaxation rate constant for
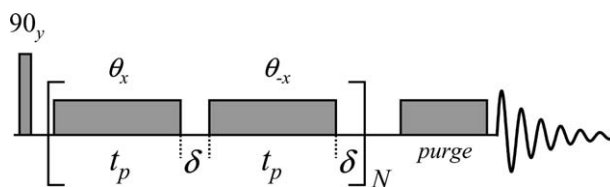

Fig. 1. An alternating-phase pulsed spin-lock sequence used to measure $R_{1\rho}^{\text{AP}}$. The length of the pulse t_p was varied from 8.5 to 498.5 μs with interpulse delay $\delta = 1.5$ μs. Purging pulse was applied with phase x and duration of 4 ms. The duration of the spin-lock period, $T = 2N(t_p + \delta)$, was up to 200 ms, corresponding to 20,000 phase-switching events in the case of "fine slicing," $t_p = 8.5$ μs.

this line under conditions of alternating-phase spin lock can be calculated using Redfield theory formalism [12] (see Appendix A for details):

$$R_{1\rho}^{AP} = p_a p_b (\Delta\omega_{ab})^2 \tau_{ex} \left[\frac{1}{1 + (\omega_1 \tau_{ex})^2} \right] f(\varphi, \theta), \qquad (3A)$$

$$f(\varphi, \theta) = 1 + \frac{2\varphi^2}{1 + \varphi^2} \frac{\cosh(\theta/\varphi) - \cos(\theta)}{(\theta/\varphi)\sinh(\theta/\varphi)}, \qquad (3B)$$

where two new variables have been introduced for brevity, $\varphi = \omega_1 \tau_{ex}$ and $\theta = \omega_1 t_p$. Angles θ and φ define, in dimensionless form, two time intervals that are important for the problem at hand. The formula Eqs. (3A) and (3B) holds for the on-resonance case where the carrier frequency is set equal to ω_{obs}. Short interpulse delays δ have been ignored in the derivation (see below).

Note that the result for $R_{1\rho}^{AP}$, Eq. (3A), has the same structure as the well-known formula for $R_{1\rho}^{CW}$, Eq. (1), with the difference expressed by the factor $f(\varphi, \theta)$. It is easy to verify that $f(\varphi, \theta) \geqslant 1$. This means that alternating-phase spin lock is less efficient in suppressing the exchange broadening than conventional spin lock of the same amplitude. The dependence of $R_{1\rho}^{AP}$ on φ and θ is illustrated in Fig. 2.

The limiting case of the continuous-wave spin lock is obtained when $\theta \gg \varphi$ ($t_p \gg \tau_{ex}$). In this limit $f(\varphi, \theta) = 1$ and $R_{1\rho}^{AP}(\varphi)$ follows the standard Lorentzian dispersion profile, Eq. (3A). It is intuitively obvious that for sufficiently long RF pulses our experiment becomes indistinguishable from the *cw* spin lock experiment. This conventional behavior is illustrated in Fig. 2 by the cross-section A.
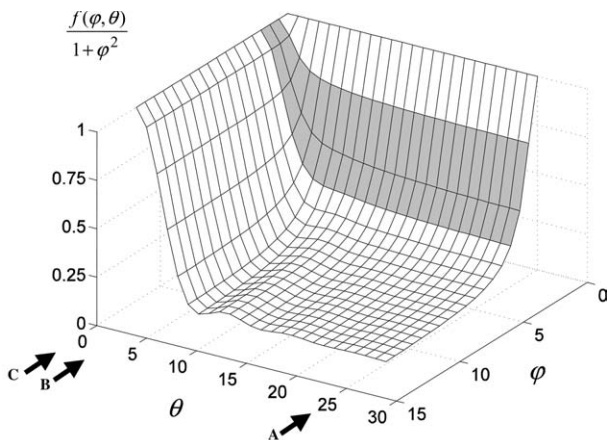

Fig. 2. A three-dimensional representation of the factor $f(\varphi, \theta)/(1 + \varphi^2)$ describing the dependence of $R_{1\rho}^{AP}$, Eqs. (3A) and (3B), on $\varphi = \omega_1 \tau_{ex}$ and $\theta = \omega_1 t_p$. The shaded region approximately corresponds to the range of φ sampled in our experimental measurements. Three different cross-sections are indicated by the arrows, including cross-section B at $\theta = 3.14(180°)$. The surface shown in the plot can also be parameterized in terms of φ and $\beta = t_p/\tau_{ex}$, cf. Eqs. (3A) and (3B). This alternative representation (not shown) is convenient for visualizing the dependence of $R_{1\rho}^{AP}$ on ω_1.

This result can be also rationalized using the following simple argument. When the value of θ is large, each individual pulse in the pulse train Fig. 1 effectively consists of a number of back-to-back 180° pulses. These 180° pulses refocus the random phase that is accrued by magnetization exchanging between the two states with different resonance frequencies [10]. The application of the RF field therefore suppresses random dephasing and eliminates line-broadening induced by chemical exchange. This effect is not different from the effect of continuous-wave spin lock. Infrequent phase-switching turns out to be unimportant in this context.

In contrast, when the value of θ dips below 180° the pulse train $(\theta_x)(\theta_{-x})(\theta_x)(\theta_{-x})\ldots$ looses its refocusing properties. For example, the pair of consecutive pulses $(5_x^\circ)(5_{-x}^\circ)$ does nothing to refocus chemical shift evolution. As a result, application of RF pulses does not prevent the dephasing of magnetization due to chemical exchange. In the limit of θ approaching zero the RF pulses become completely ineffectual and the dispersion profile is flat (cross-section C in Fig. 2). The transition between the two regimes corresponding to large and small values of θ occurs in the vicinity of $\theta = 180°$ (cross-section B in Fig. 2).

The analytical formula Eqs. (3A) and (3B) was validated using numeric simulations. For instance, we used numeric methods to generate the analogue of the surface shown in Fig. 2 (see Section 3 for details of calculations). In brief, the evolution of spin magnetization during the course of the experiment was modeled using Bloch–McConnell equation [15] involving 6×6 matrices. The simulations were carried out using the set of parameters suitable for conformational exchange in cyclohexane [6]: $p_a = p_b = 0.5$, $\Delta\omega_{ab}/(2\pi) = 250\,\text{Hz}$, $\tau_{ex} = 40\,\mu\text{s}$. Signal intensities were evaluated for $T = 0$ and $T = 60\,\text{ms}$ and used to calculate the relaxation rates, $R_{1\rho}^{AP}$. These rates were subsequently compared with the analytical results, Eqs. (3A) and (3B).

Excellent agreement was obtained between the numeric and analytical results. Over the entire range of φ and θ sampled in Fig. 2 the difference in $R_{1\rho}^{AP}$ did not exceed a small fraction of one percentage point, 0.07%. Similar negligible errors were found for other values of T in the range from 10 to 200 ms.

Fig. 2 demonstrates that the rate of phase switching represents a new control parameter that can be used to tune the effective strength of the RF field without altering the amplitude ω_1. The experiment shown in Fig. 1 has been designed to make use of this favorable property. Accordingly, further discussion focuses on the dependence of $R_{1\rho}^{AP}$ on θ (or, more specifically, the length of the pulse t_p). It is noteworthy that this dependence has distinctive shape which includes, for large values of φ, modest sinusoidal modulation (see Eqs. (3A) and (3B) and Fig. 2).

The molecule of cyclohexane was chosen as a model system to probe the effect of alternating-phase spin lock on the spin magnetization undergoing chemical exchange. Chair-to-chair transformation in cyclohexane has been extensively studied by different methods including spin-lock and CPMG experiments [6,16–18]. The transformation involves interconversion of six axial and six equatorial protons, $p_a = p_b = 0.5$, $\Delta\omega_{ab} \approx 0.5$ ppm. To avoid potential complications from homonuclear J-couplings, we choose to study the sample of deuterium-labeled cyclohexane, $C_6D_{11}H$.

Experimental relaxation rate constants $R_{1\rho}^{AP}$ measured as a function of pulse length t_p are shown in Fig. 3. The experimental data span the region of φ,θ space approximately corresponding to the shaded area in the plot of Fig. 2. The data were fitted using two or three floating parameters, as summarized in Table 1. The results are in good agreement with the values previously reported in the literature, $\Delta\omega_{ab}/(2\pi) = 253$ Hz and $\tau_{ex} = 44.5\,\mu s$, determined under the same experimental conditions [18].

The experiment shown in Fig. 1 is rather demanding with respect to the spectrometer hardware operation. In our measurements, each scan involved up to 20,000 phase-switching events. Even slight phase instability can be detrimental in this context. Using a Bruker spectrometer and pulse programming syntax (described in Section 3) we achieved a near-satisfactory performance of the sequence. In particular, a 1.5 μs interpulse delay δ was chosen as a compromise value allowing for reasonably clean phase-switching (with our spectrometer we found that shorter delays led to severe distortions whereas longer delays, up to 3.0 μs, produced no visible improvement in the quality of data). However, we were unable to completely eliminate spurious effects from rapid phase-switching. Specifically, it has been found that by the end of the spin-lock period the magnetization deviates by a small angle, less than 20°, from the direction of the locking field. The deviation was reproducible from one measurement to another and dependent on the length of the spin-lock pulse t_p. In the relaxation experiment of Fig. 1 this effect manifested itself as small pseudo-random phase distortion occurring through the series of spectra recorded with different values of N.

Since these phase distortions clearly represented instrumental artifact, we decided to erase the small component of magnetization orthogonal to the direction of the spin-lock field. With this goal in mind, we tested an extended phase-cycling scheme but did not observe any improvement. Finally, we opted for the purging pulse inserted in front of the acquisition period (note that a special pulse is needed to dephase the orthogonal component of magnetization since the pulse train in the sequence of Fig. 1 is self-compensated with respect to RF field inhomogeneity). The values of $R_{1\rho}^{AP}$ obtained with and without the purging pulse proved to be identical. However, application of the purging pulse was deemed useful since it automatically ensured proper phasing of the spectra.
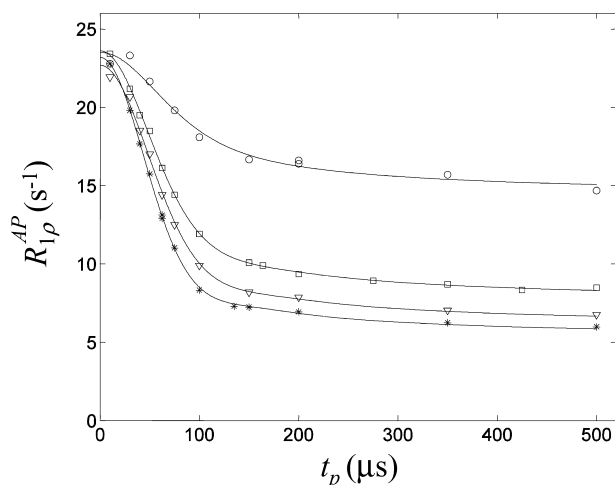

Fig. 3. Proton relaxation rate constants $R_{1\rho}^{AP}$ measured in cyclohexane $C_6D_{11}H$ using the pulse sequence Fig. 1 with different spin-lock strengths $\omega_1/(2\pi)$: ○, 3.45 kHz; □, 6.10 kHz; ▽, 6.76 kHz; and *, 7.52 kHz. The solid lines are three-parameter (τ_{ex}, $\Delta\omega_{ab}$, and ω_1) best-fit curves obtained with Eqs. (3A) and (3B). The measurements were carried out at −9 °C.

Table 1
Best-fit parameters for two-site chemical exchange in cyclohexane

	$\Delta\omega_{ab}/(2\pi)$ (Hz)[a]		$\tau_{ex}(\mu s)$[a]		$\omega_1/(2\pi)$ (kHz)[a]	
CW spin lock with variable ω_1						
	244.7 ± 0.8	—	40.1 ± 0.4	—	0–6.76	—
AP spin lock with variable t_p						
11 dB	245.4 ± 0.8	243 ± 2	39.2 ± 0.3	39.9 ± 0.5	7.52	7.41 ± 0.06
12 dB[b]	244 ± 1	233 ± 3	39.5 ± 0.6	42 ± 1	6.76	6.3 ± 0.1
	244 ± 2	235 ± 4	39.3 ± 0.7	42 ± 1		6.4 ± 0.1
13 dB	250.5 ± 0.7	250 ± 2	38.2 ± 0.3	38.3 ± 0.6	6.10	6.08 ± 0.09
18 dB	252 ± 3	260 ± 10	37 ± 1	35 ± 3	3.45	3.6 ± 0.3

[a] Left column corresponds to two-parameter (τ_{ex}, $\Delta\omega_{ab}$) fit. The strength of the RF field (indicated in the shaded area) has been determined by calibrating 360° pulse. Right column corresponds to a three-parameter (τ_{ex}, $\Delta\omega_{ab}$, and ω_1) fit, as illustrated in Fig. 3.
[b] The data from repeat measurements.

Following the application of the purging pulse, the x-projection of spin magnetization is passed for detection. The magnitude of the x-projection, however, slightly varies from one spectrum to another, which leads to pseudo-random modulation of the relaxation curves. Fig. 4 shows the data from the constant-time experiment where the duration of the spin-lock period was maintained constant, while the length of the "slice" t_p was varied. Fig. 4A shows the intensity of the TMS signal as a function of t_p. The flat profile indicates the absence of chemical exchange. Pseudo-random deviations with the amplitude of ca. 6% ($\approx 1 - \cos 20°$) are clearly seen in the graph. The data for cyclohexane are presented in

Fig. 4B. This profile can be viewed as a constant-time analogue of the curve (∇) plotted in Fig. 3 (peak intensities in Fig. 4 can be converted into relaxation rate constants in Fig. 3). The cyclohexane data show pronounced variation as a function of t_p which indicates the presence of chemical exchange. Note that pseudo-random deviations observed in this profile clearly follow the same pattern as in Fig. 4A. This confirms the instrumental origin of the effect. While we do not have a specific explanation for this behavior, we would like to emphasize that (i) it is hardware-specific and probably can be overcome using the latest-generation hardware and (ii) it does not interfere in any significant way with the measurements of chemical exchange. It is interesting to note that comparable artifacts were recently encountered (and successfully suppressed) in multiple-quantum version of CPMG experiment which does not have the self-compensating properties of the original sequence [19].

In what follows we briefly discuss the prospects for application of alternating-phase spin lock in studies of µs to ms motions in proteins. The treatment presented in this paper is limited to on-resonance case. If RF carrier frequency is different from ω_{obs} then two consecutive spin-lock pulses, θ_x and θ_{-x}, produce two effective fields that are no longer collinear. As a result magnetization travels on a complex path involving multiple cones of precession [20]. While off-resonance experiment can be analyzed along the same lines as on-resonance, the correct interpretation is predicated on the accurate knowledge of the carrier offset.

In the context of potential protein studies this problem has two aspects. First, on-resonance experiment must be performed separately for each individual peak in the spectrum. Second, the position of the RF carrier should be carefully adjusted each time to coincide with the center of the peak.

The first requirement does not necessarily constitute a serious limitation. The series of spectra with arrayed RF carrier frequency have been recorded in off-resonance spin-lock studies [21,22] and in the studies using weak spin-lock fields [23]. In most cases the number of residues affected by chemical exchange is relatively small [24,25] and the corresponding spectral peaks can be easily identified by standard methods. Hence, multiple measurements using on-resonance alternating-phase spin lock do not need to be exceedingly time-consuming.

The second requirement warrants more thorough discussion. As described above, our sequence is highly sensitive to the offset effects. In particular, the simulations indicate that even a small offset affects the shape of the relaxation profile. To investigate this effect, we simulated the relaxation dispersion curves corresponding to the constant-time experiment such as shown in Fig. 4. The data were simulated assuming the presence of a small offset and subsequently compared with the
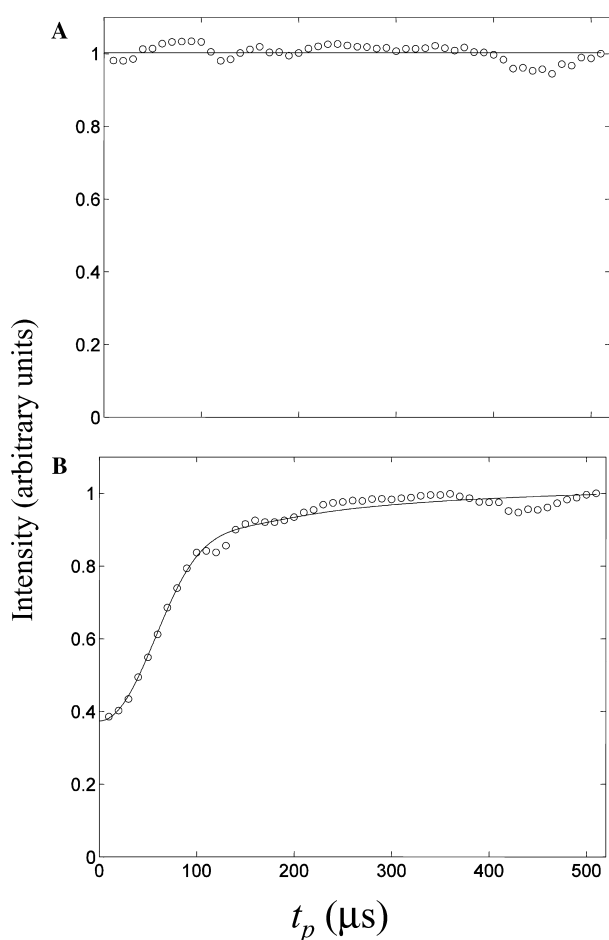

Fig. 4. Intensities of the proton spectral lines from (A) tetramethylsilane and (B) cyclohexane-d_{11} obtained using the pulse sequence Fig. 1 with $T = 60$ ms and variable pulse duration t_p. In each of the measurements, (A) and (B), the RF carrier was set on resonance with the spectral line of interest. The data were collected on a sample containing 12% of cyclohexane and 1% of TMS at proton resonance frequency 499.89 MHz, RF field strength $\omega_1/(2\pi) = 6.76$ kHz, and temperature -9 °C. Solid line in (B) corresponds to four-parameter fit with Eqs. (3A) and (3B) yielding the following best-fit values: $\tau_{ex} = 39 \pm 4$ µs, $\Delta\omega_{ab}/(2\pi) = 250 \pm 20$ Hz, and $\omega_1/(2\pi) = 6.8 \pm 0.2$ kHz (the fourth parameter that defines the intensity scale is of no interest). For comparison, a two-parameter fit of the same data yields $\tau_{ex} = 38.7 \pm 0.5$ µs and $\Delta\omega_{ab}/(2\pi) = 247.5 \pm 0.7$ Hz.

results from the on-resonance formula Eqs. (3A) and (3B). It was found that the offset of 0.3 Hz presents no problem. The deviations in the estimated relaxation rates did not exceed 0.5%. Furthermore, the fitting of the simulated data with on-resonance formula resulted in less than 0.7% error in the extracted values of $\Delta\omega_{ab}$ and τ_{ex}. However, already the offset of 1.0 Hz produced 5% error in effective $R_{1\rho}^{AP}$ rates and up to 7% errors in the best-fit parameters. Therefore, it is important to ensure that the carrier frequency is set with the accuracy of 0.3 Hz or better. In our recent experience involving mid-sized protein T4 lysozyme, it was possible to determine the resonance frequencies of the spectral peaks with the accuracy of better than 0.2 Hz [26]. The residual dipolar coupling studies typically claim precision of 1 Hz or better (in some cases as good as 0.1 Hz) [27]. Since residual dipolar couplings are usually obtained from analyzing a pair of doublets, this translates into precision of at least 0.5 Hz with regard to the position of individual peaks. We conclude therefore that it is possible to ensure the necessary precision in setting the RF field carrier even in the case of broad spectral lines. Note that special care should be taken to determine the resonance frequencies under the same heating conditions as in the alternating-phase spin lock measurements.

In the context of potential protein applications one should also mention the problem of heteronuclear J-couplings. As can be expected, scalar coupling becomes fully operational in the limit of short t_p (small θ) and strongly interferes with the results of measurements. This spurious effect can be suppressed by means of on-resonance cw decoupling. In the case of ^1H–^{13}C pair from cyclohexane, our simulations indicate that ^{13}C cw decoupling performs well starting from RF field strength of ca. 300 Hz (except for rare situations where one or two data points from the relaxation dispersion profile are affected by Hartmann–Hahn transfer).

The described experimental technique offers certain practical advantages for quantitative studies of chemical exchange. In effect, the sequence allows for adjustment of RF field strengths by varying the length of the spin-lock pulse t_p. The range of RF field strengths that can be accessed in this manner is the same as in cw spin lock experiment and superior to the CPMG sequence where high ω_1^{eff} are not available because of the sample and probe overheating.

Furthermore, the analysis of experimental data obtained with the alternating-phase spin lock experiment does not necessarily require calibration of ω_1. Instead, as shown in Table 1, ω_1 can be determined by direct fitting. This feature is reminiscent of the CPMG experiment where RF field calibration is not needed (except for hard 180° pulses). In contrast, the cw spin lock experiment is dependent on ω_1 calibration and the measured relaxation rates can be biased as discussed below [28].

In brief, when RF field is calibrated via 360° pulse the observed signal originates from both the central part of the sample (where B_1 is strong and homogeneous) and from the edges (where B_1 is weak and inhomogeneous). The RF field strength determined in this fashion represents the weighted average of these two contributions. The situation is different in multidimensional heteronuclear experiments. In these experiments signal originates almost exclusively from the central part of the sample (the response from the edges is greatly reduced because the RF field is weak in these regions and multiple hard pulses applied during the course of the sequence perform poorly). As a result, effective spin-lock strength that needs to be considered in the analyses of multidimensional experiments is several percent higher than ω_1 determined from 360° pulse calibration [29]. This discrepancy directly translates into error in τ_{ex}. To avoid this error, special calibration experiments may be required for each individual pulse sequence [28]. Our approach is free of this complication so long as ω_1 can be used as a fitting parameter (simulation results; not shown).

Finally, the new experimental scheme avoids undesirable variations in sample heating. Considering the constant-time experiment, Fig. 4, the amount of sample heating does not change with variation of t_p. On the contrary, use of the cw spin lock with variable ω_1 or the CPMG train with a variable number of pulses can produce a series of spectra corresponding to somewhat different sample temperatures. This would cause subtle, yet significant, distortions in the relaxation dispersion profiles.

Wang and Bax reported the sample heating of 3 °C in a heteronuclear two-dimensional experiment at 600 MHz proton frequency using a sample with intermediate ionic strength [30]. Furthermore, the amount of heating increases at higher magnetic fields (scales approximately quadratically with ω_0) and at higher ionic strengths. In the case of cyclohexane, 3 °C heating causes 20% reduction in τ_{ex}. Since the degree of heating varies in cw spin lock and CPMG experiments, this can be viewed as a measure of uncertainty potentially associated with these experiments.

The adverse effects of variable RF power are not limited to variations in the temperature of the sample. As recently documented by Guenneugues et al. [28], high level of RF power can cause an amplifier droop and/or detuning of resonance contour, leading to appreciable bias in dispersion profiles. The effect can be especially severe in cryogenic probes.

Wang and Bax [30] proposed the temperature compensation scheme that involves additional RF irradiation during the interscan delay. With regard to constant-time relaxation dispersion experiments, this approach means that RF power applied during the compensatory irradiation period should be adjusted a number of times to ensure that the temperature of the sample remains

unchanged throughout the series of measurements. Considering the fact that the two irradiation periods are separated in time (e.g., by evolution period t_1) it may be difficult to predict the steady-state temperature of the sample and ensure the exact compensation. Furthermore, this approach may not guard against the drooping/detuning effects mentioned above. In this respect our method that utilizes the dependence of $R_{1\rho}^{AP}$ on t_p provides an attractive alternative since it is intrinsically temperature-compensated.

In conclusion, *cw* spin lock, CPMG, AP spin lock, as well as hypothetical other experiments that probe chemical exchange using amplitude- or phase-modulated RF fields, essentially encode the same information. However, each of these experiments has its own practical advantages. Furthermore, it can be expected that an array of different experiments can provide a better handle on fine details of dynamic processes. For example, a combination of measurements may help to discriminate between different exchange regimes [31] or to identify 3-site exchange processes [32].

3. Materials and methods

499.89 MHz ^{1}H NMR measurements were carried out at $-9\,°C$ on a Bruker DRX-500 NMR spectrometer equipped with a 5 mm TBI HCX Z probe (^{1}H observe, ^{13}C and BB decoupling, z-axis gradient). The durations of 360° pulses at 0, 11, 12, 13, 15, 18 21, and 24 dB power levels were 37.3, 133, 148, 164, 205, 290, 402, and 580 μs, respectively. The sample used in this work contained 81.7% CS_2 (Aldrich), 12% $C_6D_{11}H$ (C/D/N Isotopes), 5.3% CD_2Cl_2 (Aldrich), and 1% TMS (Aldrich). The composition of the sample exactly matched that of [17,18]. All compounds were used as purchased without further purification. The sample was not degassed to avoid exceedingly long T_1 times and recycling delays. The spectrometer was locked using deuterium signal from $C_6D_{11}H$.

The alternating-phase spin lock sequence (see Fig. 1) was programmed in a number of different ways. Best results were obtained using the statement *cpds1* [33]. This command calls the external file that contains an infinite loop encoding alternating-phase pulses, θ_x and θ_{-x}, separated by service delay δ. The purging pulse was applied with the same power as spin-lock pulses and had the length of 4 ms.

Each experimental point in Fig. 3 was obtained from the complete relaxation curve (eleven different T values for each t_p setting). The shortest T used was 20 μs and the longest was approximately 200 ms. The relaxation rate constants $R_{1\rho}^{AP}$ were extracted using the program $t1/t2$ which is the part of Xwinnmr package from Bruker [34]. In the constant-time experiment, Fig. 4, T was set to 60 ms. All spectra were acquired using a single

scan and recycling delay of 100 s (approximately six times the longitudinal relaxation time, $T_1 = 16.2$ s).

The conventional *cw* spin lock measurements were carried out at power levels 12, 15, 18, 21, and 24 dB resulting in $R_{1\rho}^{CW}$ values of 6.25, 9.80, 13.6, 16.9, and 19.6 s^{-1}, respectively. In addition, $R_{1\rho}^{CW}$ value at $\omega_1 = 0$ was obtained from the measurement using a single Hahn echo (23.9 s^{-1}).

The exchange parameters, τ_{ex} and $\Delta\omega_{ab}$, together with the RF field strength, ω_1, were obtained by least-square fitting of the relaxation rate constants $R_{1\rho}^{AP}$ using the Matlab procedure *fminsearch* [35]. The data were fitted to Eqs. (3A) and (3B) neglecting small contribution ($R_2 \approx R_1 = 0.06$ s^{-1}) from relaxation mechanisms other than exchange broadening. The standard deviations in the fitted parameters were obtained from Monte Carlo simulations (1000 runs) [36].

The calculations based on Eqs. (3A) and (3B) were complemented by numeric simulations. The effect of the pulse sequence Fig. 1 was simulated using Bloch–McConnell equation [15] involving 6×6 evolution matrices for *x*-, *y*-, and *z*-components of spin magnetization exchanging between two inequivalent sites. The relaxation rate constants $R_{1\rho}^{AP}$ were evaluated from the ratio of signal intensities at $T = 0$ and 60 ms. In particular, the simulations established that the presence of the interpulse delay δ has a negligible effect (less than 0.1%) on the determined relaxation rates. Indeed, in the limit of short spin-lock pulses, $t_p = 8.5$ μs, the effect of the RF field is effectively canceled by rapid phase-switching so that the presence of idle time $\delta = 1.5$ μs with $\omega_1 = 0$ does not alter the picture. In the case of long spin-lock pulses, $t_p \cong 100$ μs, δ constitutes a small fraction of the pulse length and likewise proves to be inconsequential. Thus, Eqs. (3A) and (3B) hold very well despite the presence of the short service delays δ.

Appendix A

Consider a single spin exchanging between two non-equivalent sites, *a* and *b*. Under fast exchange conditions, $\Delta\omega_{ab}\tau_{ex} \gg 1$, a single spectral line is observed at the frequency $\omega_{obs} = p_a\omega_a + p_b\omega_b$. In the on-resonance spin lock experiment the RF carrier is set at ω_{obs}, defining thereby the rotating frame of reference. In this rotating frame the Zeeman Hamiltonian becomes:

$$H_Z(t) = \Delta\omega_{ab}n(t)I_z, \tag{A.1}$$

where $n(t)$ is a step-like random function which takes the values of p_b and $-p_a$ with the probabilities p_a and p_b, respectively. The mean value of $n(t)$ is zero, $\langle n(t)\rangle = 0$, and the correlation function is exponential, $G(\tau) = \langle n(t)n(t+\tau)\rangle = p_a p_b \exp(-|\tau|/\tau_{ex})$.

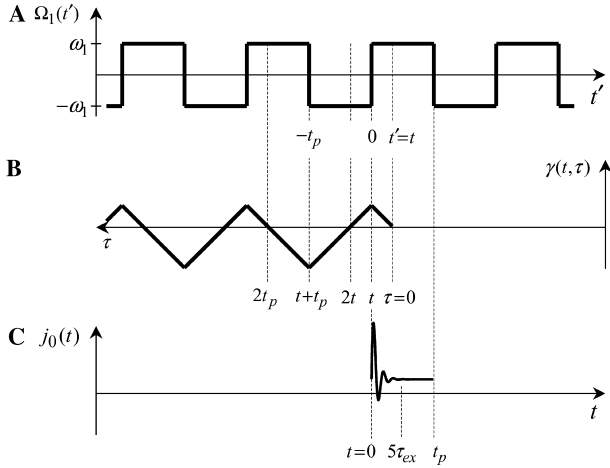The phase-alternated spin lock field in the rotating frame of reference is described by the Hamiltonian

Fig. 5. Schematic representation of the functions: $\Omega_1(t')$, Eq. (A.2); $\gamma(t,\tau)$, Eq. (A.4); and $j_0(t)$, Eq. (A.7).

$$H_{\mathrm{RF}}(t) = \Omega_1(t)I_x, \tag{A.2}$$

where the amplitude $\Omega_1(t)$ is illustrated in Fig. 5A.

The starting point in our derivation is Eq. (279) from the comprehensive work of Goldman [12], which describes the evolution of the spin-density matrix $\sigma(t)$ in the presence of an arbitrary time-dependent RF field. For the problem under consideration, this equation can be written in explicit form as follows:

$$\frac{\mathrm{d}}{\mathrm{d}t}\sigma(t) = -\mathrm{i}[\omega_{\mathrm{obs}}I_z, \sigma(t)] - p_a p_b (\Delta\omega_{ab})^2$$
$$\times \int_0^\infty \mathrm{e}^{-\tau/\tau_{\mathrm{ex}}}[I_z,[\mathrm{e}^{-\mathrm{i}\gamma(t,\tau)I_x}I_z\mathrm{e}^{\mathrm{i}\gamma(t,\tau)I_x},\sigma(t)]]\,\mathrm{d}\tau, \tag{A.3}$$

where

$$\gamma(t,\tau) = \int_{t-\tau}^t \Omega_1(t')\,\mathrm{d}t'. \tag{A.4}$$

The last term in the original Goldman formula corresponds to the equilibrium spin density matrix. It has been omitted in Eq. (A.3) since in this treatment we focus on transverse relaxation. Furthermore, we avoid the Dyson time-ordering operator since the Hamiltonian Eq. (A.2) commutes with itself at different moments in time. Based on Eq. (A.3) the relaxation rate of interest can be evaluated as:

$$R_{1\rho}^{\mathrm{AP}}(t)$$
$$= p_a p_b (\Delta\omega_{ab})^2 \int_0^\infty \mathrm{e}^{-\tau/\tau_{\mathrm{ex}}}\mathrm{Tr}\{I_x[I_z,[\mathrm{e}^{-\mathrm{i}\gamma(t,\tau)I_x}I_z\mathrm{e}^{\mathrm{i}\gamma(t,\tau)I_x},I_x]]\}$$
$$/\mathrm{Tr}\{I_xI_x\}\,\mathrm{d}\tau. \tag{A.5}$$

Note that the obtained relaxation coefficient depends on time t. Using basic spin algebra Eq. (A.5) can be simplified:

$$R_{1\rho}^{\mathrm{AP}}(t) = p_a p_b (\Delta\omega_{ab})^2 \mathrm{Re}\{K\}$$
$$= p_a p_b (\Delta\omega_{ab})^2 \int_0^\infty \mathrm{e}^{-\tau/\tau_{\mathrm{ex}}}\cos\gamma(t,\tau)\,\mathrm{d}\tau. \tag{A.6}$$

Fig. 5B shows the phase $\gamma(t,\tau)$ as a function of τ for given value of t. We shall split the domain of integration in Eq. (A.6) into the intervals $[2nt_{\mathrm{p}}, 2(n+1)t_{\mathrm{p}}]$, where n is an integer beginning with 0, and evaluate partial integrals $j_n(t) = \int_{2nt_{\mathrm{p}}}^{2(n+1)t_{\mathrm{p}}} \mathrm{e}^{-\tau/\tau_{\mathrm{ex}}}\cos\gamma(t,\tau)\,\mathrm{d}\tau$. Using the explicit form of $\gamma(t,\tau)$, see Eq. (A.4) and Fig. 5B, the integral $j_0(t)$ can be written as

$$j_0(t) = \int_0^t \mathrm{e}^{-\tau/\tau_{\mathrm{ex}}}\cos(\omega_1\tau)\,\mathrm{d}\tau$$
$$+ \int_t^{t+t_{\mathrm{p}}} \mathrm{e}^{-\tau/\tau_{\mathrm{ex}}}\cos(\omega_1(2t-\tau))\,\mathrm{d}\tau$$
$$+ \int_{t+t_{\mathrm{p}}}^{2t_{\mathrm{p}}} \mathrm{e}^{-\tau/\tau_{\mathrm{ex}}}\cos(\omega_1(2t_{\mathrm{p}}-\tau))\,\mathrm{d}\tau \tag{A.7}$$

and evaluated in a straightforward manner. This result is formulated for t in the interval from 0 to t_{p}. Since $\gamma(t,\tau)$ is periodic with respect to τ with period $2t_{\mathrm{p}}$, see Fig. 5B, $j_{n+1}(t) = \exp(-2t_{\mathrm{p}}/\tau_{\mathrm{ex}})j_n(t)$. The partial integrals, therefore, can be summed as terms of a geometric progression leading to:

$$R_{1\rho}^{\mathrm{AP}}(t) = p_a p_b (\Delta\omega_{ab})^2 \frac{1}{1-\mathrm{e}^{-2t_{\mathrm{p}}/\tau_{\mathrm{ex}}}}j_0(t). \tag{A.8}$$

Finally, we determine the effective decay rate over the interval of time t from 0 to t_{p} (indicated in Fig. 5C):

$$R_{1\rho}^{\mathrm{AP}} = p_a p_b (\Delta\omega_{ab})^2 \frac{1}{1-\mathrm{e}^{-2t_{\mathrm{p}}/\tau_{\mathrm{ex}}}}\frac{1}{t_{\mathrm{p}}}\int_0^{t_{\mathrm{p}}} j_0(t)\,\mathrm{d}t. \tag{A.9}$$

The result coincides with Eqs. (3A) and (3B) in the text. From the symmetry considerations it is obvious that the same effective decay rate $R_{1\rho}^{\mathrm{AP}}$ would be in effect for the subsequent time intervals, from t_{p} to $2t_{\mathrm{p}}$, from $2t_{\mathrm{p}}$ to $3t_{\mathrm{p}}$, etc.

The transition from Eqs. (A.8) to (A.9) warrants some additional discussion. For the sake of example we shall first consider the situation when t_{p} is substantially longer than τ_{ex}. Considering the analytical result for $j_0(t)$, Eq. (A.7), we note that it has a functional form $c_1+c_2\exp(-t/\tau_{\mathrm{ex}})\sin(\omega_1t)+c_3\exp(-t/\tau_{\mathrm{ex}})\sin(\omega_1(t_{\mathrm{p}}-t))$, where the coefficients c_k are time-independent. This function, therefore, quickly reaches the plateau. For the sake of argument, let us assume that the plateau is reached after the time $5\tau_{\mathrm{ex}}$, as illustrated in Fig. 5C.

In the rotating frame of reference, the evolution of transverse magnetization M_x is governed by

$$\frac{\mathrm{d}M_x(t)}{\mathrm{d}t} = -R_{1\rho}^{\mathrm{AP}}(t)M_x(t), \tag{A.10}$$

where $R_{1\rho}^{\mathrm{AP}}(t)$ is given by Eq. (A.8). According to the fundamental assumption of the Redfield theory, the spin observable $M_x(t)$ does not change substantially over the period of time $5\tau_{\mathrm{ex}}$ (this assumption is equivalent to the condition $\Delta\omega_{ab}\tau_{\mathrm{ex}} \gg 1$). Since the variation of $M_x(t)$ during the period of time from 0 to $5\tau_{\mathrm{ex}}$ is small, the average decay rate can be defined over this time interval according to:

$$\frac{dM_x(t)}{dt} = -\frac{1}{5\tau_{ex}} \left[\int_0^{5\tau_{ex}} R_{1\rho}^{AP}(t)\, dt \right] M_x(t). \qquad (A.11)$$

Throughout the remaining period of time, from $5\tau_{ex}$ to t_p, the function $j_0(t)$ is constant, see Fig. 5C. The relaxation rate $R_{1\rho}^{AP}(t)$, Eq. (A.8), is therefore time-independent and meets the definition of a first-order kinetics rate constant. Formally, the average rate can be defined via

$$\frac{dM_x(t)}{dt} = -\frac{1}{t_p - 5\tau_{ex}} \left[\int_{5\tau_{ex}}^{t_p} R_{1\rho}^{AP}(t)\, dt \right] M_x(t). \qquad (A.12)$$

Combining Eqs. (A.11) and (A.12) and invoking expression Eq. (A.8) for $R_{1\rho}^{AP}(t)$, we arrive at Eq. (A.9). While in this discussion we assumed that t_p is longer than τ_{ex}, the same reasoning applies for arbitrary t_p.

It is worth noting that in the above treatment the spin-lock period was assumed to be infinitely long so that potential "edge effects" associated with the finite duration of T were neglected. This is the standard feature of Redfield theory that also can be traced to the assumption that the evolution of spin observables is negligible on a time scale of τ_{ex}. The derivation presented here is valid in the case of fast chemical exchange. Different perturbation treatments are available to treat the case of intermediate or slow exchange (cf. [37]).

References

[1] R. Ishima, D.I. Freedberg, Y.-X. Wang, J.M. Louis, D.A. Torchia, Flap opening and dimer-interface flexibility in the free and inhibitor-bound HIV protease and their implications for function, Structure 7 (1999) 1047–1055.

[2] A. Malmendal, J. Evenäs, S. Forsén, M. Akke, Structural dynamics in the C-terminal domain of calmodulin at low calcium levels, J. Mol. Biol. 293 (1999) 883–899.

[3] R.B. Hill, C. Bracken, W.F. DeGrado, A.G. Palmer, Molecular motions and protein folding: characterization of the backbone dynamics and folding equilibrium of α_2D using ^{13}C NMR spin relaxation, J. Am. Chem. Soc. 122 (2000) 11610–11619.

[4] E.Z. Eisenmesser, D.A. Bosco, M. Akke, D. Kern, Enzyme dynamics during catalysis, Science 295 (2002) 1520–1523.

[5] G. Binsch, A unified theory of exchange effects on nuclear magnetic resonance lineshapes, J. Am. Chem. Soc. 91 (1969) 1304–1309.

[6] C. Deverell, R.E. Morgan, J.H. Strange, Studies of chemical exchange by nuclear magnetic relaxation in the rotating frame, Mol. Phys. 18 (1970) 553–559.

[7] H. Wennerström, Nuclear magnetic relaxation induced by chemical exchange, Mol. Phys. 24 (1972) 69–80.

[8] K. Kloiber, R. Konrat, Differential multiple-quantum relaxation arising from cross-correlated time-modulation of isotropic chemical shifts, J. Biomol. NMR 18 (2000) 33–42.

[9] Z. Luz, S. Meiboom, Nuclear magnetic resonance (NMR) study of the protolysis of trimethylammonium ion in aqueous solution—order of the reaction with respect to solvent, J. Chem. Phys. 39 (1963) 366–370.

[10] M. Bloom, L.W. Reeves, E.J. Wells, Spin echoes and chemical exchange, J. Chem. Phys. 42 (1965) 1615–1624.

[11] R. Konrat, M. Tollinger, Heteronuclear relaxation in time-dependent spin systems: ^{15}N-T_ρ dispersion during adiabatic fast passage, J. Biomol. NMR 13 (1999) 213–221.

[12] M. Goldman, Formal theory of spin-lattice relaxation, J. Magn. Reson. 149 (2001) 160–187.

[13] J.B. Grutzner, R.E. Santini, Coherent broad-band decoupling—an alternative to proton noise decoupling in carbon-13 NMR spectroscopy, J. Magn. Reson. 19 (1975) 173–187.

[14] M.H. Levitt, Heteronuclear cross polarization in liquid-state nuclear magnetic resonance: mismatch compensation and relaxation behavior, J. Chem. Phys. 94 (1991) 30–38.

[15] H.M. McConnell, Reaction rates by nuclear magnetic resonance, J. Chem. Phys. 28 (1958) 430–431.

[16] E. Juaristi, Conformational behavior of six-membered rings: analysis, dynamics, and stereoelectronic effects, VCH, New York, 1995.

[17] F.A.L. Anet, A.J.R. Bourn, Nuclear magnetic resonance line-shape and double-resonance studies of ring inversion in cyclohexane-d_{11}, J. Am. Chem. Soc. 89 (1967) 760–768.

[18] Y.S. Wang, S. Ikuta, Accuracy of molecular dynamics obtained by $T_{1\rho}$ measurements on the microsecond time scale in solution, Magn. Reson. Chem. 27 (1989) 1134–1141.

[19] V.Y. Orekhov, D.M. Korzhnev, L.E. Kay, Double- and zero-quantum NMR relaxation dispersion experiments sampling millisecond time scale dynamics in proteins, J. Am. Chem. Soc. 126 (2004) 1886–1891.

[20] The non-trivial evolution of magnetization arises from $-i[H, \sigma(t)]$ term in the master equation for spin density matrix where the Hamiltonian H includes time-averaged Zeeman interaction and off-resonance RF field with alternating phase.

[21] S. Zinn-Justin, P. Berthault, M. Guennegues, H. Desvaux, Off-resonance rf fields in heteronuclear NMR: application to the study of slow motions, J. Biomol. NMR 10 (1997) 363–372.

[22] D.M. Korzhnev, V.Y. Orekhov, F.W. Dahlquist, L.E. Kay, Off-resonance $R_{1\rho}$ relaxation outside of the fast exchange limit: an experimental study of a cavity mutant of T4 lysozyme, J. Biomol. NMR 26 (2003) 39–48.

[23] F. Massi, E. Johnson, C. Wang, M. Rance, A.G. Palmer, NMR $R_{1\rho}$ rotating-frame relaxation with weak radio frequency fields, J. Am. Chem. Soc. 126 (2004) 2247–2256.

[24] F.A.A. Mulder, A. Mittermaier, B. Hon, F.W. Dahlquist, L.E. Kay, Studying excited states of proteins by NMR spectroscopy, Nat. Struct. Biol. 8 (2001) 932–935.

[25] M.J. Grey, C. Wang, A.G. Palmer, Disulfide bond isomerization in basic pancreatic trypsin inhibitor: multisite chemical exchange quantified by CPMG relaxation dispersion and chemical shift modelling, J. Am. Chem. Soc. 125 (2003) 14324–14335.

[26] N.R. Skrynnikov, F.W. Dahlquist, L.E. Kay, Reconstructing NMR spectra of "invisible" excited protein states using HSQC and HMQC experiments, J. Am. Chem. Soc. 124 (2002) 12352–12360.

[27] A. Bax, Weak alignment offers new NMR opportunities to study protein structure and dynamics, Protein Sci. 12 (2003) 1–16.

[28] M. Guenneugues, P. Berthault, H. Desvaux, A method for determining B_1 field inhomogeneity. Are the biases assumed in heteronuclear relaxation experiments usually underestimated?, J. Magn. Reson. 136 (1999) 118–126.

[29] F.J.M. van de Ven, Multidimensional NMR in Liquids, VCH, New York, 1995.

[30] A.C. Wang, A. Bax, Minimizing the effects of radio-frequency heating in multidimensional NMR experiments, J. Biomol. NMR 3 (1993) 715–720.

[31] O. Millet, J.P. Loria, C.D. Kroenke, M. Pons, A.G. Palmer, The static magnetic field dependence of chemical exchange

linebroadening defines the NMR chemical shift time scale, J. Am. Chem. Soc. 122 (2000) 2867–2877.

[32] D.M. Korzhnev, X. Salvatella, M. Vendruscolo, A.A. Di Nardo, A.R. Davidson, C.M. Dobson, L.E. Kay, Characterizing low populated folding intermediates of an SH3 domain by NMR spectroscopy (submitted).

[33] NMR Suite. Pulse Program Reference Manual. Bruker BioSpin GmbH, 2002.

[34] NMR Suite. Processing Reference Manual, Bruker BioSpin GmbH, 2003.

[35] Using MATLAB, The MathWorks Inc, 2001.

[36] P.R. Bevington, D.K. Robinson, Data Reduction and Error Analysis for the Physical Sciences, McGraw-Hill Inc, New York, 1992.

[37] O. Trott, A.G. Palmer, $R_{1\rho}$ relaxation outside of the fast-exchange limit, J. Magn. Reson. 154 (2002) 157–160.